J. Fluid Mech. (1977), *vol.* 80, *part* 3, *pp.* 535–559
Printed in Great Britain

Effects of water waves on the structure of turbulent shear flow

By K. TAKEUCHI,
Department of Civil Engineering, Stanford University, Stanford, California 94305†
E. LEAVITT
AIDJEX, University of Washington, Seattle
AND S. P. CHAO
Department of Civil Engineering, Stanford University, Stanford, California 94305‡

(Received 16 June 1975 and in revised form 3 September 1976)

The structure of the turbulent shear flow over a propagating wave of fixed frequency is examined. The vertical and horizontal velocities were measured in a wind–wave facility at Stanford University. The structure of the wave-perturbed turbulence was found to depend significantly on the ratio of the local mean velocity to the wave speed. The results support the idea of 'cat's-eye' type flow about the mean critical height.

1. Introduction

Water waves and their interactions with turbulent shear flows have been intriguing subjects for observation and speculation for many years. Much of the theoretical work in this field is related to problems of wave generation and wave growth mechanisms based on extensions of the work of Miles and Phillips. Many experimental investigations have been undertaken but their results show considerable disagreement between theories and observation. With the advent of high-speed computers and the advancement of numerical techniques, the most recent approach to these problems consists of constructing numerical flow models. The work by Davis (1970), Townsend (1972) and Norris & Reynolds (1975) is representative of this approach. Numerical models require some type of closure assumption for the turbulent shear stresses and the lack of complete experimental data exerts a restraining influence on progress. As was pointed out by Davis (1970), the problem of wave generation cannot be solved until the wave's influence on the turbulent shear flow is understood.

The structure of the turbulent boundary layer in the absence of waves is fairly well understood. The visual studies of turbulent shear flows by Corino & Brodkey (1969) and Kim, Kline & Reynolds (1971) revealed the salient features of Reynolds-stress production in the wall region of the boundary layer. Using the conditional sampling technique introduced by Kovasznay, Kibens & Blackwelder (1970), Lu & Willmarth (1973) and Brodkey, Wallace & Eckelmann (1974) have reported in detail on the velocity field in wall-bounded shear flows.

† Present address: Lockheed-Georgia Company, Department 72–76, Marietta, Georgia 30063.
‡ Present address: Bechtel Corporation, San Francisco, Ca.

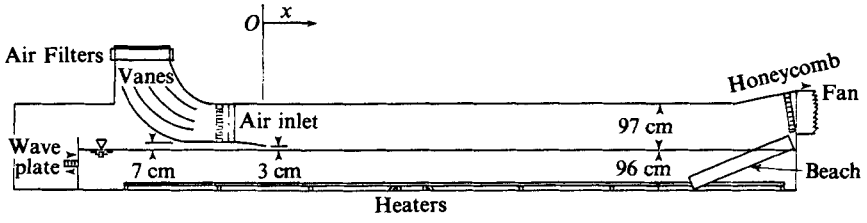

FIGURE 1. Schematic diagram of the Stanford wind–wave facility.

There have, of course, been many measurements in the laboratory of the air flow over waves. Kendall (1970) described measurements of the pressure and velocity fields over a wavy wall consisting of a smooth rubber sheet mechanically deformed into sinusoidal waves. His results showed some of the influence of waves on the turbulent flow structure. Stewart (1970) made a detailed study of wave-induced velocity fields by using artificially generated waves. Chang, Plate & Hidy (1971) measured the turbulent motion over wind-generated water waves; their measurements of local mean velocity profiles and spectra show considerable alteration of the turbulence owing to the waves. Lai & Shemdin (1971) concentrated on establishing the degree of wind–wave interaction in terms of various spectral measurements. Both Stewart (1970) and Lai & Shemdin (1971) dealt mainly with the behaviour of the wave-induced fluctuations rather than the pure turbulent velocities.

The present paper describes a series of measurements of the velocity field in the boundary layer over progressive water waves made at Stanford University. The study is restricted to mechanically generated water waves, over which the velocity fluctuations and the wave heights were measured from a platform fixed relative to the mean water surface. In this respect the study is similar to that of Stewart (1970); however more attention was paid here to the turbulence fluctuations over the waves. The influence of the waves on the velocity field is explored by comparisons with studies of turbulent flow over smooth boundaries, as well as with other data of a similar nature.

2. The experiment

The experiment was conducted in the Stanford University wind–wave facility described by Hsu (1965): figure 1 shows the main features of the wind–wave channel. When this channel is filled with water to a depth of 1 m, the air flow test section remaining is approximately 20 m long, 1 m wide and 1 m high. The cross-sectional distribution of air flow in the channel reported by Hsu indicates that the flow is two-dimensional throughout almost the entire test length.

A mechanical wave generator capable of generating selected wave forms is located at the upstream end of the channel. A beach of rectangular baskets filled with steel turnings absorbs the waves at the downstream end of the channel. Air is drawn through the test section by a suction fan located at the downstream end of the channel. The air inlet, situated approximately 3 m downstream of the wave-generating plate, contains a honeycomb 10 cm thick and a group of screens to reduce the initial turbulence. To ensure smooth air flow into the channel, a 2 m long flat plate is placed at the end of the air inlet section. The dynamic features of the channel with respect to mechanically

generated waves are reported by Bole & Hsu (1969). The wave reflexion coefficient for waves of frequency 1 Hz was found to be about 5 %.

The velocity measurement station was located approximately 13 m from the air inlet, where the average depth of the boundary layer was approximately 30 cm. All measurements were made with the velocity probe mounted on a traverse which could be fixed at prescribed heights above the mean water level. Data were taken at 20 fixed heights between 3·2 and 34 cm above the mean level for 10 values of the free-stream velocity ranging from 1·5 to 5 m s^{-1}. All measurements were made over mechanically generated waves of frequency 1 Hz and amplitude 2·5 cm. The speed C of these waves is 1·55 m s^{-1}. Different data runs are identified by double numbers such as 5–8. The first number distinguishes the different free-stream velocities and the second number the different measurement heights.

The fluctuating velocity components were detected using a quartz-coated cross hot-film probe of diameter 0·005 cm and length 0·1016 cm and Thermo-Systems, Inc. constant-temperature anemometers. The hot-film sensor was calibrated in the core or uniform flow region of the wind–wave channel immediately before and after each run. There was a long period of calibration stability for the films used, and generally the difference between any two successive calibrations was less than 3 %.

The alignment of the cross-film with respect to the mean flow was checked by rotating the sensor through 180° about the centre-line and performing an additional calibration. Generally, the computed tilt angle was less than $\pm 1°$. The output signals from the anemometers were appropriately amplified and low-pass filtered with Rockland 1022F filters with the cut-off frequency set at 500 Hz. Wave heights were measured using a capacitance-type gauge. The output of the wave gauge is a voltage linearly proportional to the immersion length. The signals from the two hot-film channels and the wave gauges were sampled every 0·001 s and stored on tape for later analysis using the computer system described in Takeuchi & Mogel (1975).

Velocities above the waves consist of a mean, a wave-induced perturbation, and a turbulent component. A phase-averaging technique was employed to extract the wave-induced fluctuations from the total signals. The instantaneous velocity field is written in component form as

$$u_i = U_i + \tilde{u}_i + u_i', \quad i = 1, 2, 3, \tag{1}$$

where U_i is the time-averaged mean velocity, $\tilde{u}_i$ is the wave-induced perturbation and u_i' is the turbulent fluctuation. The phase average is defined by

$$\langle u_i(x,t)\rangle = \lim_{N\to\infty} \frac{1}{N} \sum_{n=0}^{N} u_i(x, t+nT). \tag{2}$$

Here T is the period of the perturbation. This yields

$$\langle u_i\rangle = U_i + \tilde{u}_i \tag{3}$$

since by definition $\langle u_i'\rangle = 0$, and the turbulent fluctuation can be obtained from

$$u_i' = u_i - \langle u_i\rangle.$$

The first step in the analysis consisted of playing back the data tapes and recording the times at which the water waves had zero displacement from the mean water level and a positive slope. With the sampling rate used, each wave period contained

Run	U_∞ (m s^{-1})	U_i (m s^{-1})	U_∞/C	U_i/C	Re $\times 10^4$	y/δ	y^+	$(\overline{u'^2})^{\frac{1}{2}}$ (m s^{-1})	$(\overline{v'^2})^{\frac{1}{2}}$ (m s^{-1})	$-\overline{u'v'}$ $\times 10^{-4}$ (m^2 s^{-2})
1–1	1·33	0·945	0·86	0·61	3·68	0·085	169·7	0·105	0·0264	4·09
1–2	1·33	0·988	0·86	0·64	3·68	0·098	195·7	0·098	0·0271	5·87
1–4	1·33	1·05	0·86	0·68	3·68	0·12	256·7	0·094	0·0275	5·88
1–8	1·33	1·14	0·86	0·74	3·68	0·18	377·0	0·080	0·0270	5·29
1–10	1·33	1·18	0·86	0·76	3·68	0·23	466·9	0·076	0·0262	5·07
3–1	1·70	1·26	1·1	0·81	3·94	0·09	196·7	0·116	0·0335	7·43
5–1	2·01	1·39	1·3	0·896	4·98	0·113	307·5	0·142	0·0449	12·6
5–3	2·01	1·43	1·3	0·922	4·98	0·14	377·7	0·132	0·0455	11·79
5–5	2·01	1·47	1·3	0·948	4·98	0·18	477·0	0·133	0·0465	14·56
5–7	2·01	1·53	1·3	0·987	4·98	0·21	578·0	0·130	0·0471	13·74
5–9	2·01	1·57	1·3	1·012	4·98	0·25	680·0	0·124	0·0464	13·65
5–11	2·01	1·67	1·3	1·077	4·98	0·32	881·0	0·119	0·0466	13·65
5–13	2·01	1·76	1·3	1·135	4·98	0·4	1082·0	0·112	0·0445	12·98
5–15	2·01	1·79	1·3	1·394	4·98	0·47	1285·0	0·105	0·0425	10·57
5–17	2·01	1·87	1·3	1·206	4·98	0·58	1588·0	0·0876	0·0394	6·52
5–19	2·01	1·98	1·3	1·278	4·98	0·95	2595·0	0·0537	0·030	1·402
7–1	2·48	1·58	1·6	1·02	4·08	0·13	285·7	0·170	0·0560	18·9
7–2	2·48	1·63	1·6	1·05	4·08	0·15	316·9	0·165	0·0585	21·0
7–4	2·48	1·71	1·6	1·10	4·08	0·19	405·2	0·163	0·0612	22·7
7–6	2·48	1·77	1·6	1·14	4·08	0·24	511·7	0·160	0·0626	23·7
7–8	2·48	1·82	1·6	1·17	4·08	0·29	620·8	0·157	0·0623	22·5
7–10	2·48	1·92	1·6	1·24	4·08	0·39	836·4	0·150	0·0617	21·2
9–1	2·79	2·16	1·8	1·39	5·91	0·10	303·4	0·211	0·078	62·3
11–1	3·25	2·33	2·1	1·50	7·37	0·10	392·0	0·240	0·0886	72·4
17–1	4·43	2·94	2·86	1·90	9·29	0·11	599·0	0·358	0·130	75·7
17–2	4·43	3·05	2·86	1·97	9·29	0·13	703·0	0·346	0·127	73·6
17–4	4·43	3·26	2·86	2·10	9·29	0·17	922·0	0·324	0·123	58·3
17–6	4·43	3·37	2·86	2·17	9·29	0·21	1136·0	0·315	0·120	56·9
17–8	4·43	3·48	2·86	2·24	9·29	0·25	1355·0	0·291	0·116	50·6
17–10	4·43	3·58	2·86	2·31	9·29	0·31	1679·0	0·258	0·114	49·0

TABLE 1. Mean flow characteristics. U_∞ = free-stream velocity, U_i = local mean velocity, $Re = U_\infty \delta/\nu$, δ = boundary-layer thickness, $y^+ = yu_*/\nu$, y measured from mean water level.

approximately 1000 points and the maximum variation in the wave period (the interval between two successive zero crossings) was 1 %. The zero crossings were then used to control phase averaging of the velocity signals [equation (2)]. Each run was about 300 s long, so that 300 wave periods are included in each phase-averaged signal. For the phase averaging, the wave period was subdivided into 200 equal divisions so that each data point plotted as a function of wave phase is an average of 1500 samples and the mean values for each run are the averages of 300 000 points. Mean flow statistics of the 30 runs selected for analysis are summarized in table 1.

3. General characteristics of the flow field

3.1. *Mean profiles*

Representative dimensionless mean velocity profiles are plotted in figure 2. The non-dimensional height $y^+ = yu_*/\nu$ is measured from the mean water level. Here ν is the kinematic viscosity and $u_* = (\tau_0/\rho)^{\frac{1}{2}}$ is the shear velocity, τ_0 being the surface shear

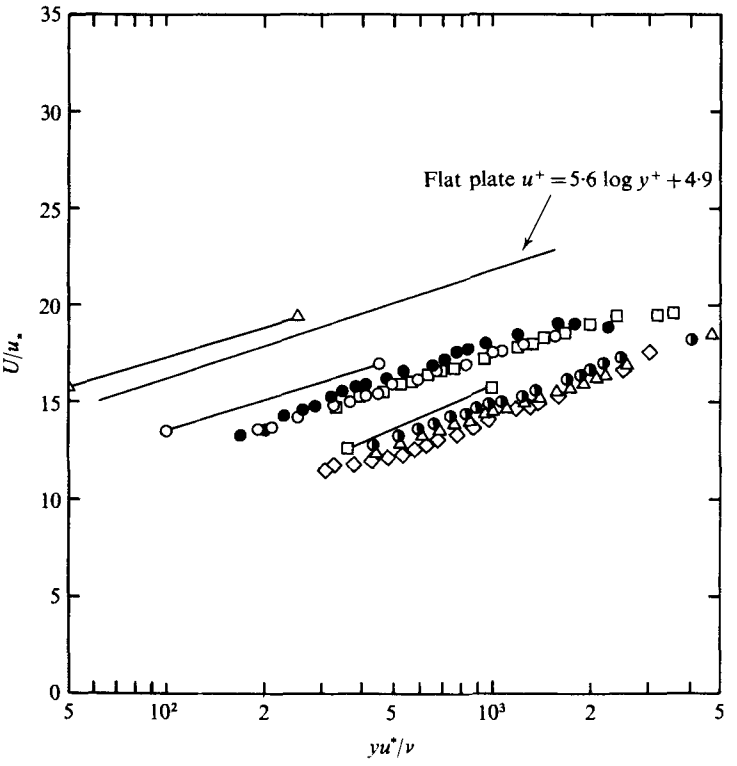

FIGURE 2. Mean velocity profiles. ●, run 1; ○, run 3; □, run 5; ◑, run 9; △, run 11; ◇, run 13. Wind-wave data from McIntosh *et al.*: △—△, $U_\infty = 2\,\mathrm{m\,s^{-1}}$; ○—○, $U_\infty = 3\,\mathrm{m\,s^{-1}}$; □—□, $U_\infty = 5\,\mathrm{m\,s^{-1}}$.

stress and ρ the density of air. Because the sensing probe is fixed at a prescribed position, the actual height above the water surface depends on the phase of the wave. For example, the value of y^+ at the lowest measurement level of run 1 varied from 39 over a crest to 320 over a trough. However, the velocity profiles still appear to vary logarithmically with height, except at the outer edge of the boundary layer.

The shear velocities were determined by a least-squares fit of the mean velocity *vs.* the logarithm of the height. This follows from the well-known law of the wall (cf. Clauser 1956)

$$U/u_* = k^{-1} \ln y^+ + C_1 - \Delta U/u_*.$$

Here k is von Kármán's constant, assumed equal to 0·4, C_1 is the flat-plate velocity defect and $\Delta U/u_*$ is the velocity defect over rough boundaries. Young, Hsu & Street (1973) found $C_1 = 4{\cdot}9$ in the Stanford wind tunnel.

Also included in figure 2 are measurements made by McIntosh, Street & Hsu (1975) over wind-generated waves for approximately the same range of wind speeds. Differences in the observed velocity defects between the two sets are relatively small. With the exception of run 5 (the u_* value of which seems to be overestimated owing to anomalous curvature in the lower three or four points) the profiles appear to cluster into two groups. It is possible that the grouping is related to the onset of rippling on the mechanical wave. Lai & Shemdin (1971), who made a similar set of measurements

Run	u_* Profile (m s^{-1})	u_* $(\overline{u'w'})^{\frac{1}{2}}$ (m s^{-1})
1	0·06	0·02
3	0·09	0·03
5	0·11	0·04
7	0·13	0·045
9	0·14	0·08
11	0·17	0·085
17	0·26	0·09

TABLE 2. Comparison of measured shear velocities.

in a different wind–wave facility, reported that u_* values computed from profiles for the same U_∞ increased when a mechanical wave was introduced (the increase being proportional to the wind speed). Lai & Shemdin's wave was 8·9 cm high with an approximate frequency of 1·5 Hz. McIntosh *et al.* report mixed results from similar wind speeds when mechanical waves are introduced. They tested two different mechanical waves of amplitude 5 cm, one of frequency 0·8 Hz and the other of frequency 1·4 Hz. The higher frequency wave seemed to increase the apparent roughness over the equivalent wind–wave case, whereas the lower frequency wave left it unchanged or caused a decrease. The 5 cm high 1 Hz wave would be expected, therefore, to have only a small effect (less than 20 %) on the observed mean profile as compared with the equivalent wind–wave case.

In wall-bounded turbulent flows the shear velocity u_* is often compared with the measured turbulent Reynolds stress in forming the surface shear stress. The relation is given by

$$\tau_0 = -\rho_a \overline{u'v'} = \rho_a u_*^2.$$

The present measurements of these quantities are summarized in table 2. The values of u_* obtained by the profile technique are seen to be 2–3 times larger than the turbulence data. The equivalence of turbulent Reynolds stress to u_*^2 is valid only in the inertial subrange (cf. Tennekes & Lumley 1972, p. 156). As will be seen in the next section, our spectra measurements show that the flow investigated has practically no inertial subrange and therefore equivalence of the shear velocity to the turbulent Reynolds stress may not be valid for this case.

The measurements of the same quantities made by Chao & Hsu (1976) with wave-following probes, however, show approximately equal values of u_*^2 and $\overline{u'v'}$. They employed essentially the same techniques and procedures as those used in this experiment. This difference between the present fixed-probe measurements of turbulent Reynolds stress and those obtained with wave-following probes by Chao & Hsu suggests the existence of unique features in the boundary layer above the progressing waves. The legitimacy of equating u_*^2 with $\overline{u'v'}$, especially for fixed-probe measurements above waves, requires further study.

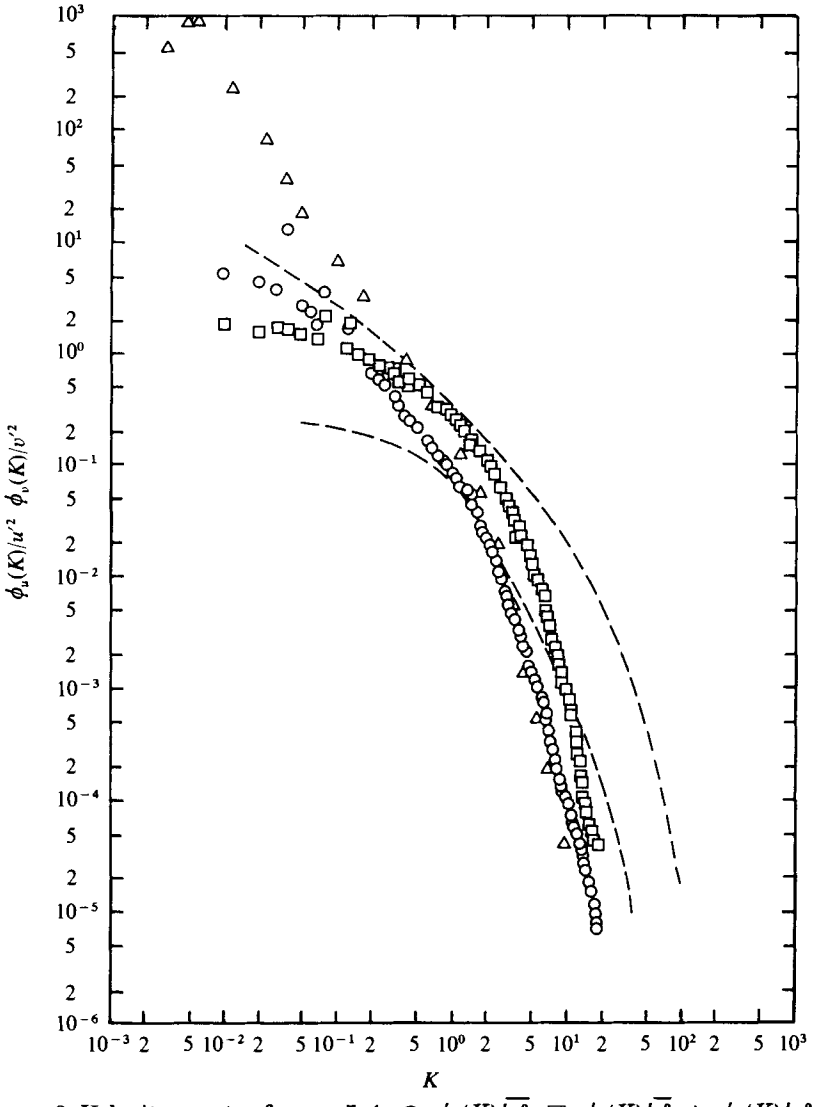

FIGURE 3. Velocity spectra for run 7–1: ○, $\phi_u(K)/\overline{u^2}$; □, $\phi_v(K)/\overline{v^2}$. △, $\phi_u(K)/u^2$ from Pond *et al.*; – – –, Klebanoff's (1954) data range.

3.2. *Velocity spectra*

Spectra of the longitudinal and vertical velocity fluctuations from run 7–1 are shown in figure 3. The spectra are presented versus the wavenumber deduced assuming Taylor's hypothesis. The ratio of the local mean velocity to the wave speed was approximately 1. The Reynolds number based on the free-stream velocity U_∞ and the boundary-layer thickness δ of 30 cm is $R_\delta = 4{\cdot}08 \times 10^4$. The thickness δ is the height where $U = 0{\cdot}99U_\infty$. The Kolmogorov microscale can be estimated to be approximately 0·01 cm using the relation $\eta = \delta/R_\delta^{\frac{3}{4}}$. Accordingly, the hot film (of length 0·1 cm) was too long to sense the behaviour in the high wavenumber region where viscous effects are expected to dominate. The turbulent Reynolds number, defined by $R_\lambda = \sigma_u \lambda/\nu$, where

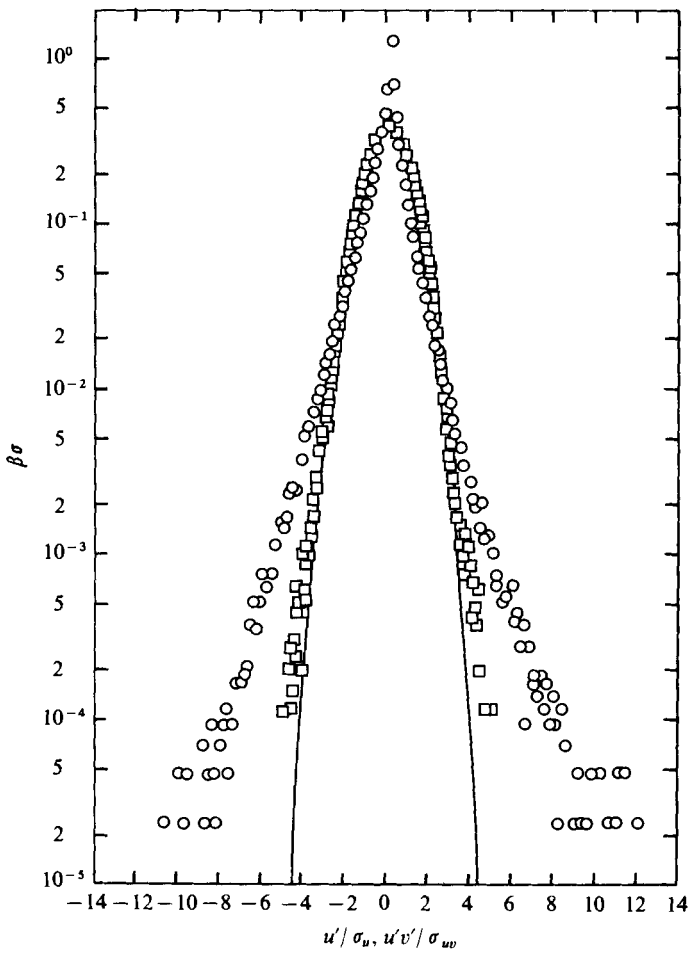

FIGURE 4. Probability distributions of u' and $u'v'$ for run 17–1. ——, Gaussian; □, u'; ○, $u'v'$. The probability density is non-dimensionalized by the appropriate standard deviation.

λ is the Taylor microscale and $\sigma_u = (\overline{u'^2})^{\frac{1}{2}}$, was approximately 10. Because of the small Reynolds number, no inertial subrange is expected. Although there is a frequency band where a $-\frac{5}{3}$ slope can be seen in the u spectra, this is not a true indication of the existence of an inertial subrange since the v spectra do not attain the required ratio of $\frac{4}{3}$ to the u spectra in this frequency band.

For comparison the band of data taken over a smooth flat plate by Klebanoff (1954) and also u spectral measurements made over ocean waves by Pond, Stewart & Burling (1963) have been included in figure 3. To reproduce the data of Pond *et al.* $\overline{u^2}$ was obtained by graphical integration of their spectra. Our results are comparable to those of Pond *et al.* except that the field data contain more energy at low wavenumbers. The deviation of the present results from those of Klebanoff is assumed to be due to the difference in Reynolds number between the two experiments.

The u spectra exhibit a large peak at 1 Hz and a smaller peak at 2 Hz, whereas the v spectra exhibit a peak only at 2 Hz. No peaks attributable to wave effects were observable in the data of Pond *et al.* or in similar measurements made over water

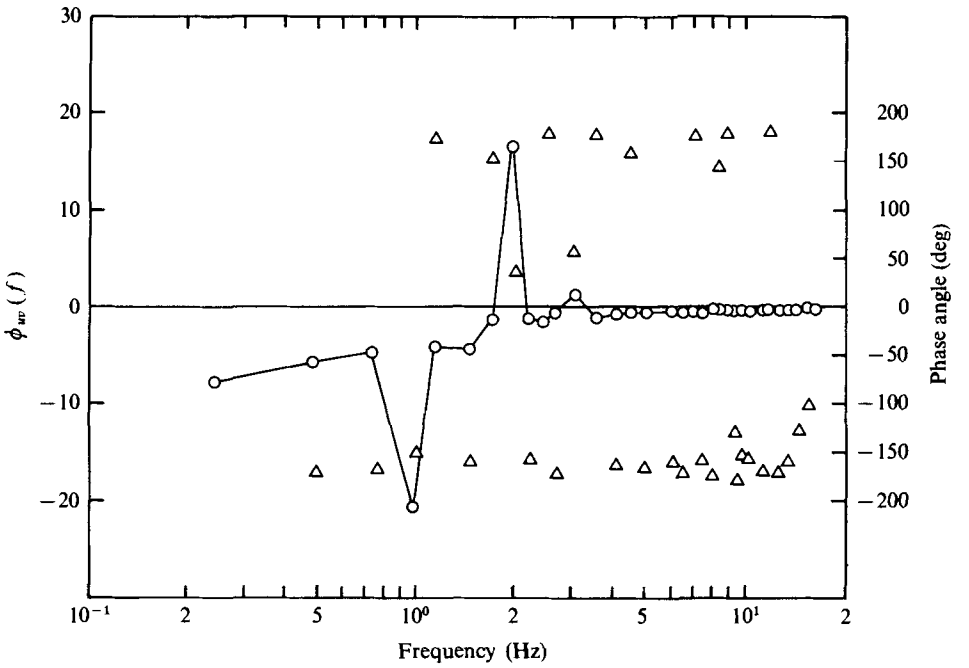

FIGURE 5. Cospectrum of u and v and phase angle for run 7–1. ○, $\phi_{uv}(f)$; △, phase angle.

waves by Smith (1967). However, field measurements by Kondo, Fujinawa & Naito (1972) and Benilov, Kouznetsov & Panin (1974) clearly show peaks at the dominant wave frequency. Lai & Shemdin's (1971) laboratory data also showed peaks in the u and v spectra at the frequency of their mechanical waves. McIntosh *et al.* (1975), in laboratory studies over wind-generated waves, also found spectral peaks at the dominant wave frequency, the peak being more noticeable in the v spectra. The absence of a peak in the v spectra for run 7–1 at the wave frequency was an effect limited to cases where $U_l/C \simeq 1$; otherwise the spectra were very similar to those of Lai & Shemdin.

The u, v cospectrum and phase for run 7–1 are plotted in figure 5. For the most part, the phase between the u and v components is $180 \pm 30°$ except at the second and third harmonics of the wave, where the cospectrum indicates upward momentum transport. The 1 Hz peak in the u spectrum is represented by a positive spike in the cospectrum. Lai & Shemdin noted positive peaks when $U_l/C < 1$ and a large negative peak when $U_l/C > 1$. Again $U_l \simeq C$ appears to represent some kind of transition between the two extremes. The question of the sign of the cospectrum peaks at the wave harmonics will be discussed again in a later section.

3.3. *Probability density and higher-order moments*

The distribution of the probability densities of the turbulent longitudinal velocity and of the turbulent Reynolds stress for run 17–1 were calculated and the results are shown in figure 4. Phase averaging has been used to remove the wave perturbations. Each probability density is normalized such that the area under the curve is unity. The solid line represents a Gaussian distribution having the same mean and standard

Run	Skewness			Kurtosis		
	u'	v'	$u'v'$	u'	v'	$u'v'$
1–1	−0·157	0·132	−0·465	3·26	3·55	10·30
1–2	−0·278	0·122	−0·919	3·22	3·27	10·08
1–4	−0·106	0·130	−0·786	2·94	3·34	10·72
1–8	−0·149	0·151	−0·936	2·89	3·35	9·70
3–1	−0·106	0·145	−0·669	3·08	3·43	10·44
7–1	−0·0151	−0·0035	−0·964	3·34	3·65	11·85
7–2	0·024	0·0002	−1·21	3·08	3·43	11·79
7–4	0·021	0·036	−0·844	3·06	3·42	10·45
7–6	0·0147	0·053	−0·800	2·96	3·29	10·24
7–8	−0·049	0·103	−0·727	3·02	3·24	9·35
7–10	−0·135	0·173	−0·885	2·94	3·23	9·78
17–1	−0·139	0·189	−0·269	2·95	3·46	10·56
17–2	−0·158	0·220	−0·428	2·74	3·44	10·69
17–4	−0·209	0·227	−0·482	2·75	3·43	9·87
17–6	−0·261	0·218	−0·585	2·84	3·44	10·54
17–8	−0·307	0·239	−0·556	2·83	3·44	11·07
17–10	−0·350	0·309	−0·582	2·95	3·55	12·10

TABLE 3. Higher-order moments.

deviation as the signal. The behaviour of the longitudinal turbulent velocity is quite close to Gaussian up to three times the standard deviation of the signal. The distribution of the vertical velocity fluctuations greater than 3σ deviates from Gaussian; otherwise its probability distribution shows essentially the same behaviour as that of u. The probability density of the Reynolds stress, however, shows considerable non-Gaussian behaviour.

The shapes of each probability density distribution are reflected in the higher-order moments summarized in table 3. The skewness is the non-dimensionalized third moment and is a measure of the symmetry of the probability density curve. A Gaussian variable has a skewness of zero and a kurtosis of three. The high kurtosis observed in the Reynolds-stress signals implies that the Reynolds-stress production is intermittent in nature, a well-known phenomenon in smooth boundary-layer flows. It is noted that u' and $u'v'$ have consistently negative skewness while v' shows positive skewness in most cases. A sudden drop in u' and v' skewness is observed in run 7–1, in which the fluctuation occurred at the mean critical height. This drop in skewness is gradually regained as the distance above the critical height is increased. The product $u'v'$ has very high kurtosis and is strongly skewed. The average kurtosis is about 10.

Probabilities and other mean statistics are very similar to results found in smooth boundary-layer flows. The present results agree especially well with the findings of Gupta & Kaplan (1972), who reported the variation of the skewness and kurtosis of u', v' and $u'v'$ as a function of distance above a smooth wall. In the range of y^+ reported in the present work they found consistently negative skewness for u' and positive skewness for v'. The kurtosis values were slightly less than three for u' and slightly larger than three for v' in this range. The average skewness values for $u'v'$ which they reported were larger ($\sim -1{\cdot}0$) and the average kurtosis values, like ours, were found to be about 10.

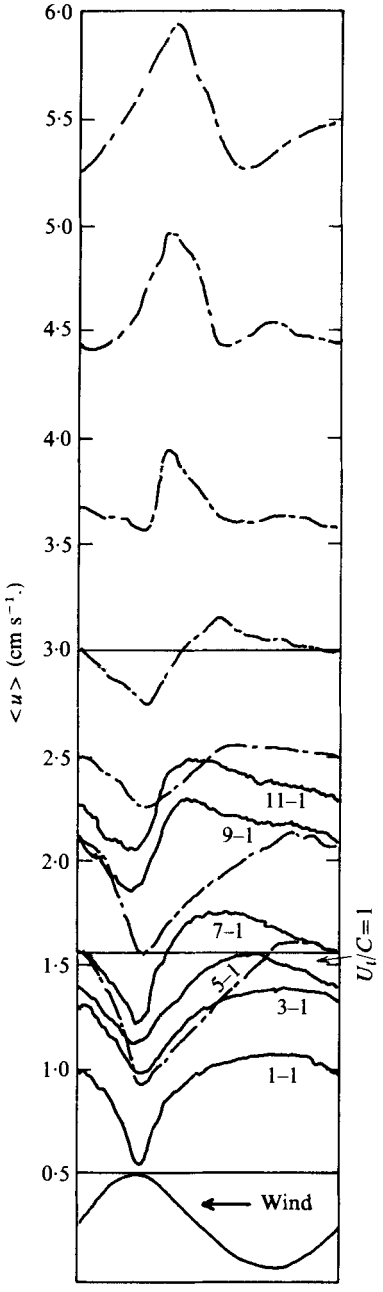

FIGURE 6

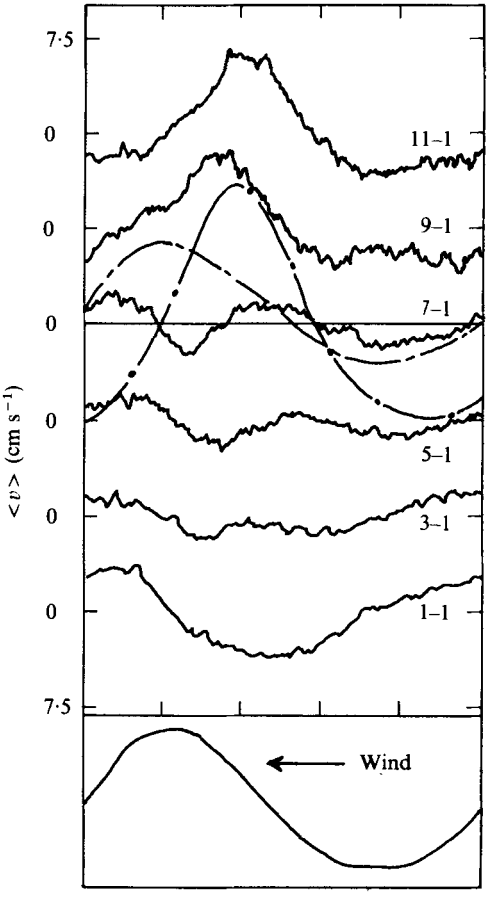

FIGURE 7

FIGURE 6. Variation of $\langle u \rangle$ with increasing U_∞ at 3·2 cm above mean water level. $U_l = C$ is indicated in the figure. —·—, measurements by Kendall (1970), for which $C = 3$ m/s. The wave phase is indicated at the bottom of the figure.

FIGURE 7. Variation of $\langle v \rangle$ with increasing U_∞ at 3·2 cm above mean water level. Kendall's (1970) data: —●—, $U_\infty/C = 2{\cdot}5$; —·—, $U_\infty/C = 1{\cdot}33$.

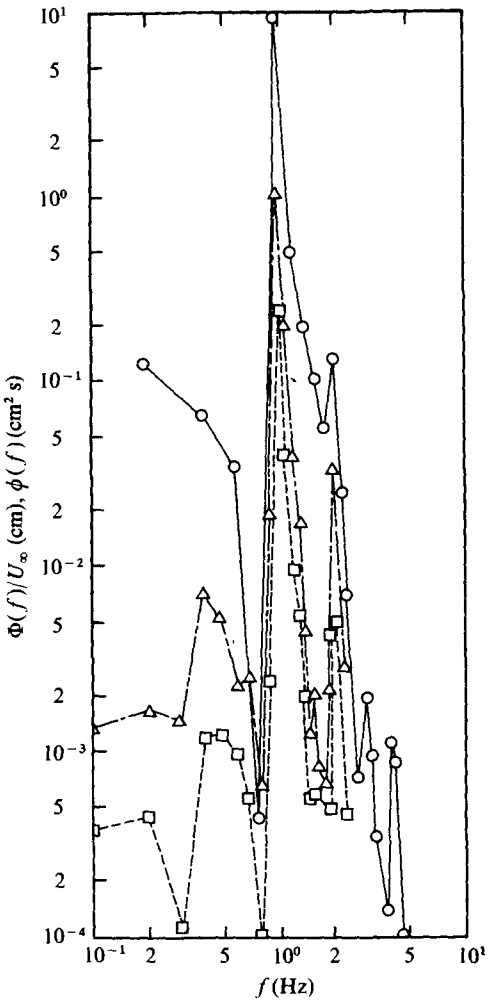

FIGURE 8. Spectra of the wave and the wave-induced velocities for run 9–1. ○, $\phi_{\eta\eta}(f)$; △, $\Phi_{\tilde{u}}(f)/U_\infty$; □, $\Phi_{\tilde{v}}(f)/U_\infty$.

Since the probability and statistics are calculated from time averages or equivalently by ensemble averaging (ergodicity assumed) of the variables, the detailed behaviour of the fluctuations tends to be lost during the averaging process (see, for example, Lahey & Kline 1971). No significant wave effects are seen in the results of statistics computed by ordinary time averaging.

4. Results and discussion

4.1. *Wave-perturbed velocity fluctuations*

Figure 6 shows the phase-averaged longitudinal velocity fluctuations $U+\tilde{u}$ for increasing values of U_l/C at a height of 3·2 cm above the mean water level. The phase averaging is described in § 2. A wave profile has been included in figure 6 to illustrate the relation between the phase of $\tilde{u}$ and the wave phase. Kendall's (1970) measurements

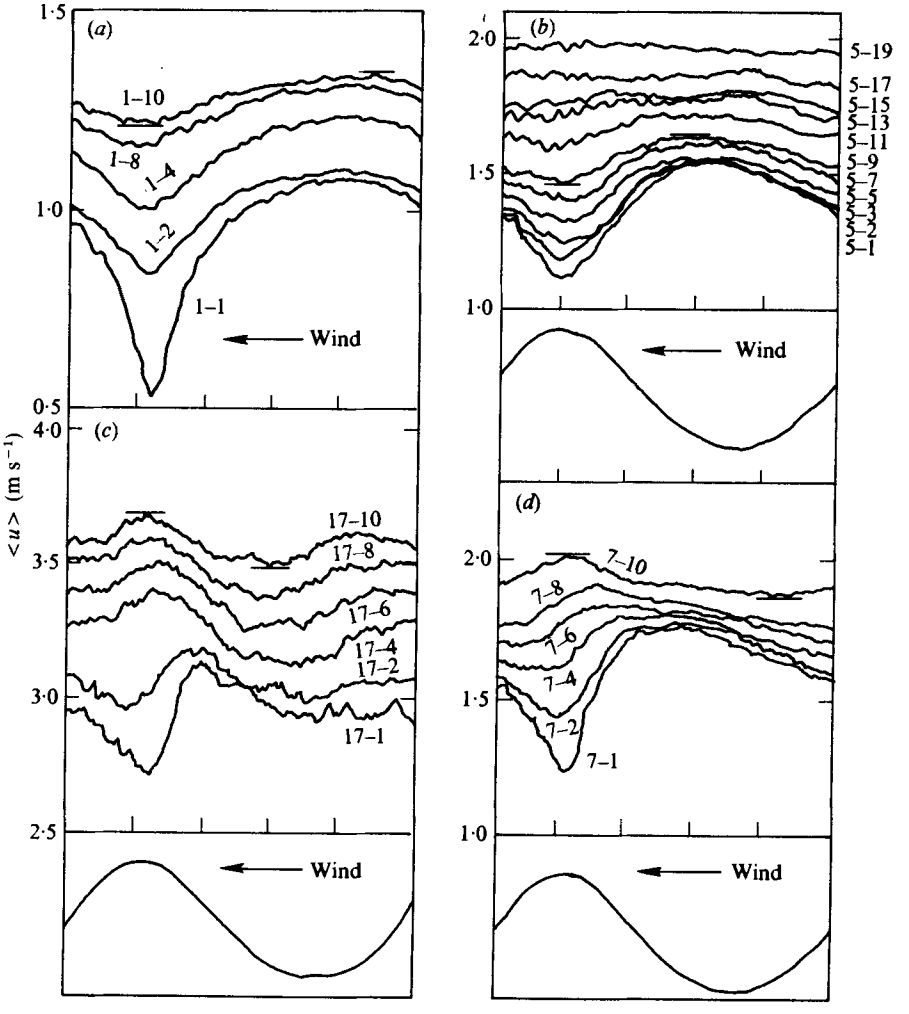

FIGURE 9. Variation in $\langle u \rangle$ with height. (*a*) Runs 1. (*b*) Runs 5. (*c*) Runs 17. (*d*) Runs 7.

are also included in the figure. The general shape of the variation is similar to Kendall's results.

The absolute amplitudes of the $\tilde{u}$ fluctuations are fairly constant for this range of velocities. In run 7–1 ($U_l/C \simeq 1$) the fluctuations are occurring across the mean critical layer. For runs 1–1, 3–1 and 5–1, $U_l/C < 1$ and measurements were made below the mean critical height; for runs 9–1 and 11–1, $U_l/C > 1$ and the measurement levels are above the mean critical height. The windward slopes of $\tilde{u}$ for the last two runs are steeper than the windward slopes of $\tilde{u}$ for the first three runs. The phase difference between the 1 Hz components of $\tilde{u}$ and the wave also changes, from 180° for run 1–1 to 140° for run 11–1.

The departure of $\tilde{u}$ from a sinusoidal form can be explained if an approximately logarithmic mean profile of the longitudinal velocity exists above the water surface at all points along the wave profile. Since measurements over a crest are closer to the

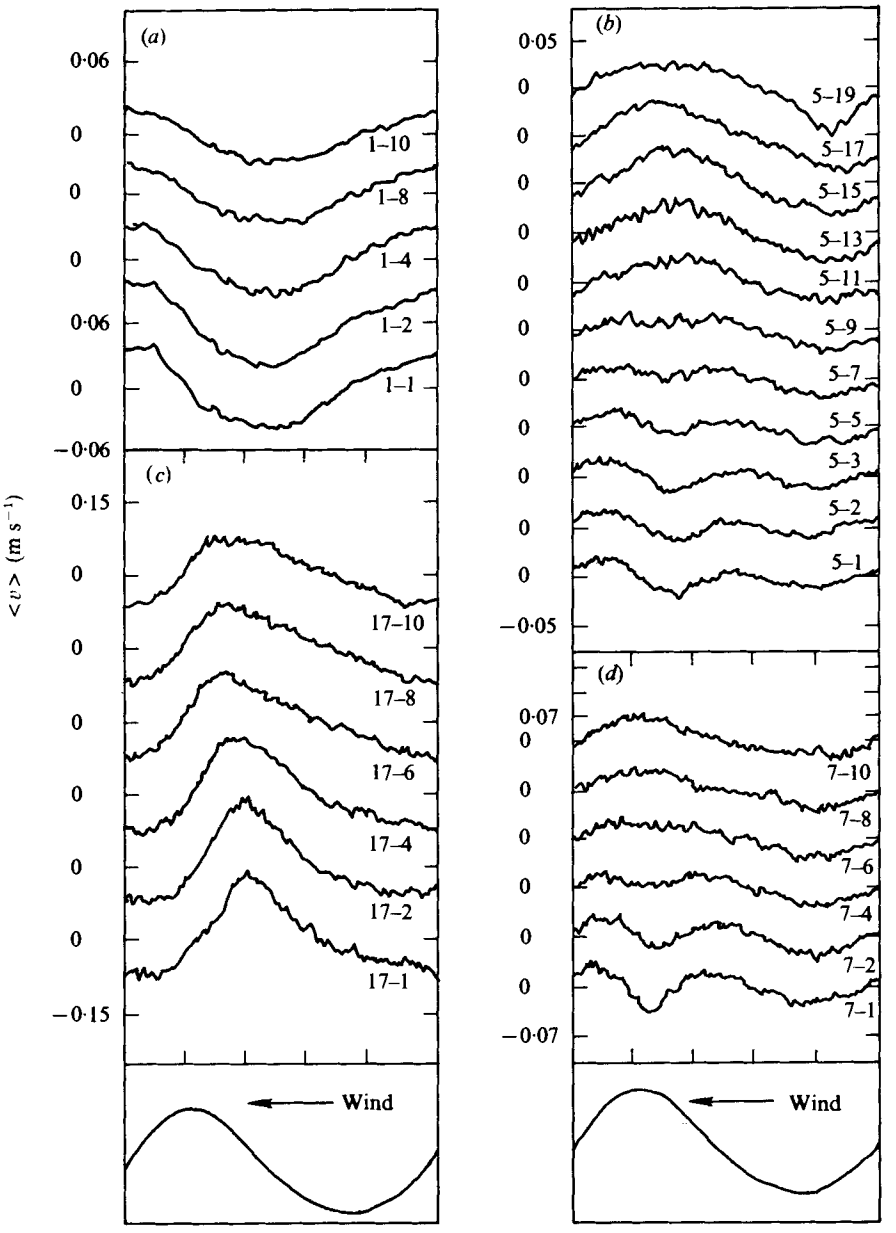

FIGURE 10. Variation in $\langle v \rangle$ with height for same runs as in figure 9.

surface than those made over a trough (by the wave height of 5 cm), $\tilde{u}$ shows a greater variation with equal changes in wave phase over a crest than over a trough. The change in the windward slopes of $\tilde{u}$ are strongly suggestive of the asymmetric pattern for flow near the critical height described by Stewart (1974). He suggests that the flow pattern becomes asymmetric if diffusion of vorticity is assumed. This would imply a loss of vorticity in the upper part of the flow to the lower part and serve as a mechanism for causing the pressure field to be out of phase with the displacement.

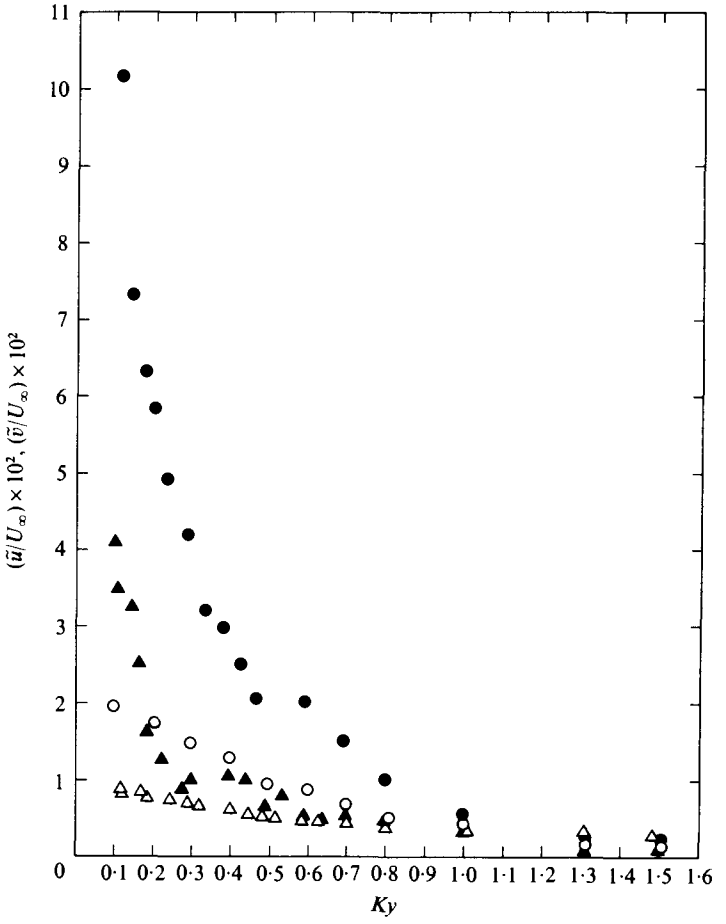

FIGURE 11. Decay of wave-induced velocities with height in the boundary layer. Closed symbols, $\tilde{u}$; open symbols, $\tilde{v}$. ○, $U_\infty/C = 0{\cdot}86$; △, $U_\infty/C = 1{\cdot}8$. y is measured from crest.

The variation of the wave-perturbed vertical velocity as a function of wave phase is presented in figure 7. Kendall's measurements are also included. Fluctuations in $\tilde{v}$ show greater changes in relative phase than the $\tilde{u}$ fluctuations. Runs 5–1 and 7–1 exhibit a frequency twice that of the water wave, hence the spectrum of the vertical velocity fluctuations for run 7–1 lacked a peak at the fundamental wave frequency. This double frequency variation appears because the sensing probe is fixed in space: hence it spends part of its time above the critical height and part below. This reasoning assumes that the critical height is fixed relative to the actual water surface as suggested by Stewart (1974).

One of the reviewers suggested that the phase reversals might be due to the influence of the higher harmonic components of the wave. In order to see what effect the higher harmonics of the wave frequency had on the wave-induced velocity fluctuations, auto-spectrum analysis was done on the wave signal with the velocity components. The results are shown in figure 8 with the wave-induced velocity spectra normalized by the free-stream velocity. The results show the existence of higher harmonics, but their

amplitudes are more than an order of magnitude smaller than that of the fundamental. The phase differences were essentially constant throughout the frequency range investigated and it is unlikely that the distinct phase changes observed are due to contributions by higher harmonics of the wind–wave interaction.

Figure 9 shows the variation of the phase-averaged $\tilde{u}$ fluctuations with height for four different wind speeds. For all cases the amplitude of $\tilde{u}$ decreases as the distance from the surface increases. Figures 9(*a*) and (*c*) illustrate the different variations for a low wind (run 1) and a moderately high wind (run 17) respectively. For run 1 the critical height is located above all the measurement stations while for run 17 the opposite is true. No significant change in the fluctuation pattern except for amplitude occurs in run 1, whereas in runs 17 and 7 a distinct phase change is observed in $\tilde{u}$ as the height above the surface increases.

In their study of turbulence over waves, Lai & Shemdin computed u and v spectra for two different wind speeds (1·95 and 10·66 m s^{-1}) at three different heights (10, 20 and 50 cm) above the mean water level. They concluded that the wave-induced velocity fluctuations decayed faster with height at the higher wind speed. They also observed that the spectral peak at the wave frequency increased with wind speed if the height was held constant.

As noted, the situation for the present data set is somewhat different. Measurements of the amplitude of $\tilde{u}$ at the lowest height showed little variation with wind speed. This also seems to be true for level 10 of each run as illustrated in figure 9. Both run 1–10 and run 17–10 have the same amplitude in $\tilde{u}$ while the $\tilde{u}$'s of runs 5–10 and 7–10 have a slightly smaller amplitude. The situation for $\tilde{v}$ (see figure 10) is different from that for the longitudinal velocity. Here things are complicated by the appearance of a double harmonic in runs 5 and 7, but in general the amplitude of $\tilde{v}$ increases with wind speed.

Figure 11 is a plot of the amplitude of $\tilde{u}$ and $\tilde{v}$ normalized by the free-stream velocity plotted against the dimensionless height Ky, where $K = 2\pi/\lambda$, λ being the wavelength of the surface wave. Two cases are presented: $U_\infty/C = 0{\cdot}86$ and $U_\infty/C = 1{\cdot}8$. In dimensionless terms the $\tilde{u}$ and $\tilde{v}$ amplitudes at the lower wind speed are larger than those at the higher wind speed. For Ky less than 0·8 the decay rates seem to be equal in contrast to Lai & Shemdin's conclusions. Higher in the boundary layer this may not be true, but the amplitudes are too small for a conclusive answer.

Kendall (1970) and Chang *et al.* (1971) also measured the longitudinal velocity, with wave-following probes. Kendall's results, for mechanical waves, indicate a maximum in $\tilde{u}$ at the wave crests and a minimum in the troughs, the amplitude of which increases with wind speed. The resulting $\tilde{u}$ is very similar to the $\tilde{u}$ profile shown for run 17–8 or 17–10. There is no phase shift with height in his u data. The measurements of Chang *et al.* were made above wind-generated waves and also showed a peak in the mean wind over the crests of the dominant waves. In their data, however, the critical layer was in the viscous sublayer and so direct comparison with the present results must be cautious.

4.2. *Turbulent velocities*

Phase analysis was also performed on the turbulent velocities. Figure 12 shows the variance of the longitudinal and vertical velocities as a function of wave phase and wind speed. They are normalized by the average turbulent variance of each variable. Measurements by Kendall are also included in this figure.

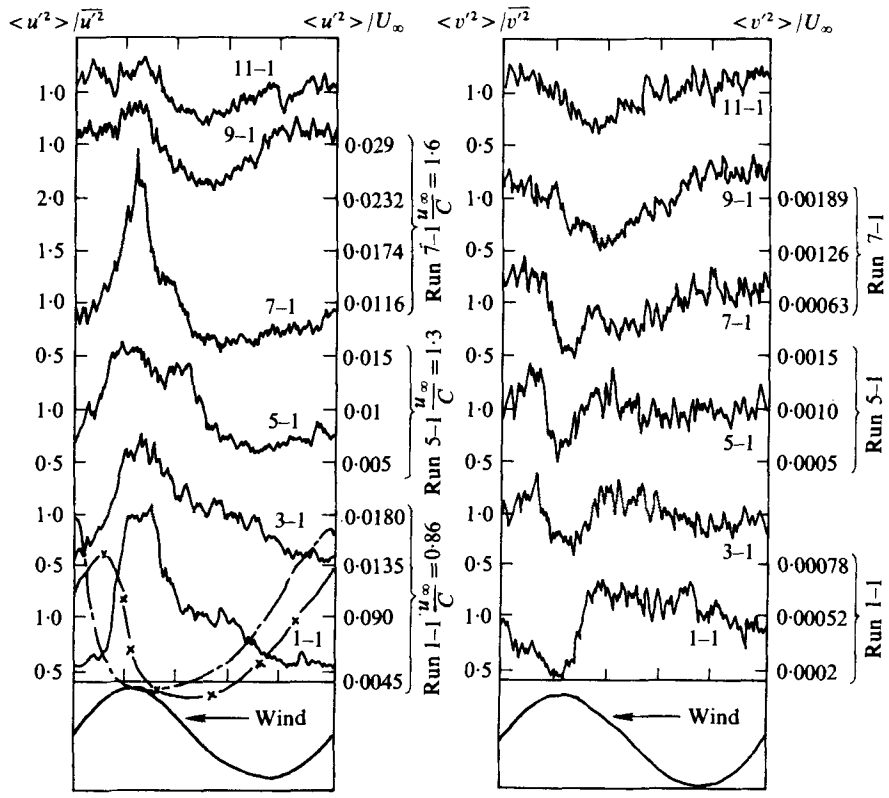

FIGURE 12. Variation in $\langle u'^2\rangle$ and $\langle v'^2\rangle$ with U_∞ at 3·2 cm above the mean water level. Kendall's (1970) data were taken with a wave-following probe. —·—, $U_\infty/C = 18{\cdot}3$; — × —, $U_\infty/C = 4{\cdot}6$.

There is a concentration of $\langle u'^2\rangle$ over the crests, especially for cases where $U_l/C \leqslant 1$. For these measurements the energy peak over the crests ranges from 1·5 to 3 times the average $\overline{u'^2}$ values while above the mean critical height the peaks decrease to nearer the average value. The region of higher turbulent intensity over the crest occurs because at that point the sensor probe is located closest to the flow boundary, where the mean intensity is higher. The downwind phase shift of the peak of $\langle u'^2\rangle$ with increasing U_∞/C observed by Kendall with his wave-following probe is not seen.

The variations in the vertical turbulent energy differ from those of the longitudinal component. A minimum in the vertical energy, which is located nearly over the wave crests in runs 1–1 to 7–1, is shifted upwind as U_∞/C becomes greater than unity. The minimum over the crests seen in figure 11 might not be expected because here the sensor is closest to the surface, where the turbulence intensity is expected to be greater.

The variation of the phase-averaged turbulent Reynolds stress normalized by its mean value is presented in figure 13. The most obvious feature is the large negative Reynolds stress occurring over the crests in run 1–1. This distinct feature disappears as the mean velocity increases, although a minimum in $\langle u'v'\rangle$ upwind of the crests is still observable. The largest contributions to the Reynolds stresses occur downwind of the crests, where the magnitude of this peak is approximately twice the average stress. Kendall's measurements from a fixed probe show similar results except that the

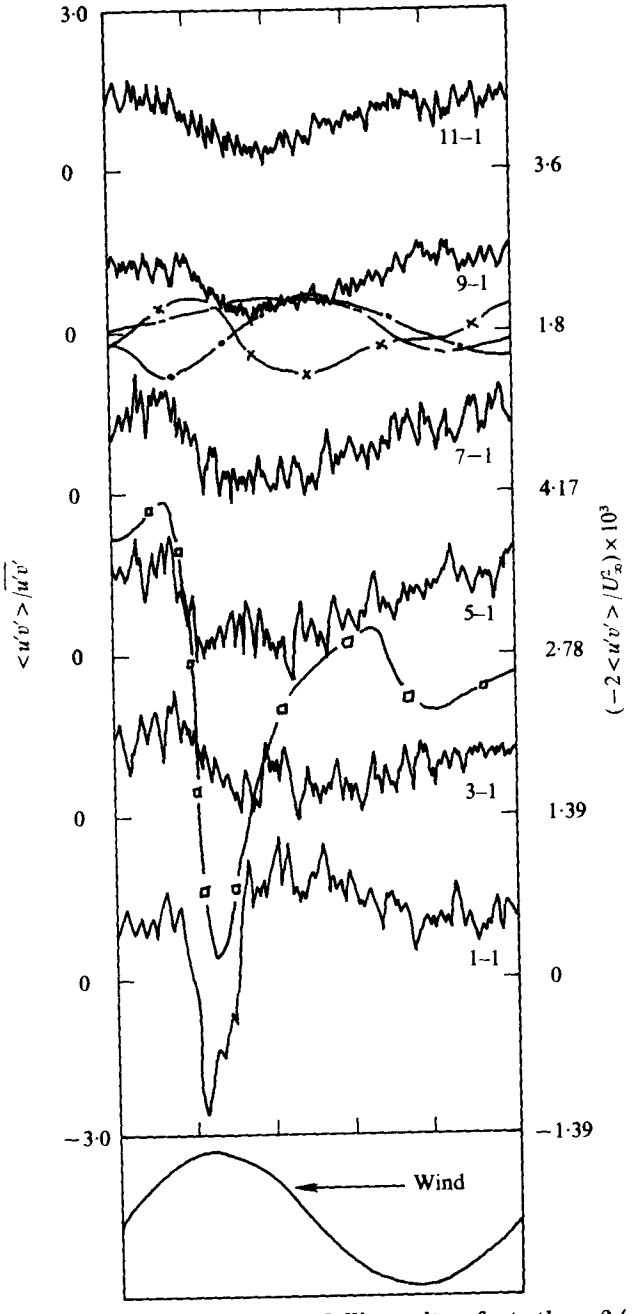

FIGURE 13. Variation in $\langle u'v' \rangle$ with U_∞. For Kendall's results refer to the $-2\langle u'v' \rangle / U_\infty$ co-ordinate. For $y = 0{\cdot}15$ cm above crest: —□—, $U_\infty/C = 4{\cdot}6$. For $y = 0{\cdot}64$ cm above crest: — · —, $U_\infty/C = 9{\cdot}6$; –●–, $U_\infty/C = 4{\cdot}7$; — × —, $U_\infty/C = 1{\cdot}84$.

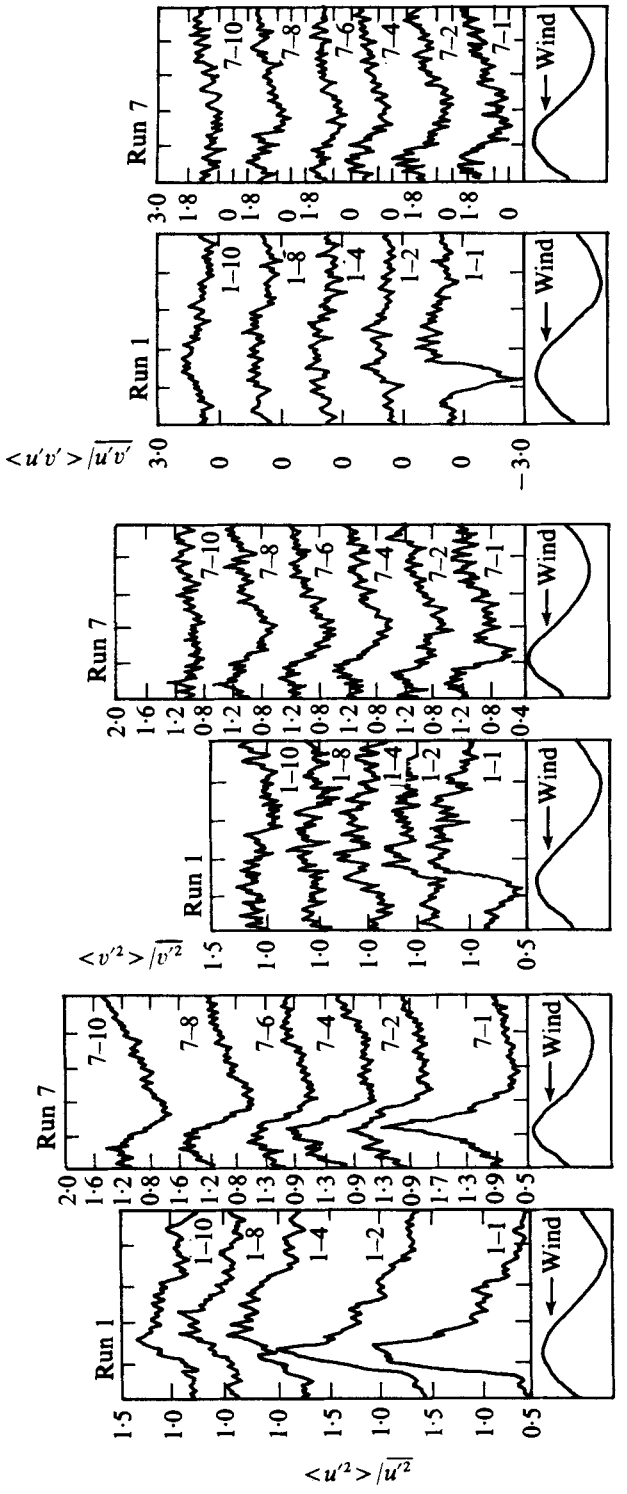

FIGURE 14. Variation in $\langle u'^2 \rangle$, $\langle v'^2 \rangle$ and $\langle u'v' \rangle$ with height for runs 1 and 7.

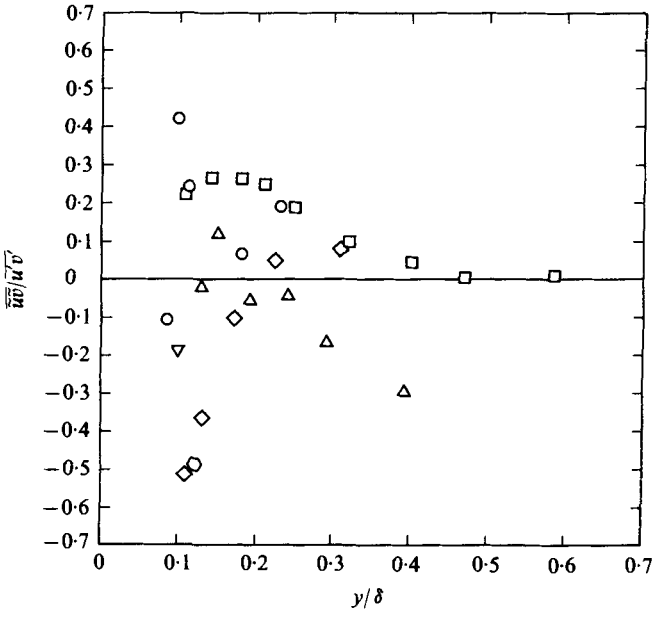

FIGURE 15. Variation in the wave-induced Reynolds stress $\tilde{u}\tilde{v}/\overline{u'v'}$ with height. Runs below the critical height: ○, 1; □, 5. Runs above the critical height: △, 7; ▽, 11–1; ◇, 17; ⬡, 19–1.

minimum $\langle u'v' \rangle$ shifts downwind with increasing height as U_∞/C increases beyond the range of the present data. At the lowest measurement height, however, his results do indicate a minimum in $\langle u'v' \rangle$ upwind of the wave crests for the reported range of U_∞/C.

If stress is considered to be the product of an eddy viscosity and the gradient of the mean velocity profile, run 1–1 implies the existence of a local negative gradient near the crests. The measurements of the local mean velocity profile by Chang *et al.* did show a negative gradient in the mean velocity profile over the crests. They attributed this to the presence of a small jet in the flow in the region of the crests.

Typical variations of the turbulent products with height are shown in figure 14. It is interesting to note that the variation of $\langle u'v' \rangle$ and $\langle v' \rangle$ is very similar, especially when U_∞/C is greater than 1.

The cyclic variation in the measured $\langle u'v' \rangle$ could be due to variation of either u' or v' or to variation in the correlation between the two. Kendall suggested that variations in the correlation were the cause of the cyclic variation. His experiment did not include calculation of v', but our measurements suggest that variations in u' and v' intensities caused the cyclic variation in $\langle u'v' \rangle$.

Values of $-\overline{\tilde{u}\tilde{v}}$, the wave-induced Reynolds stress, were also computed. Results for $\overline{\tilde{u}\tilde{v}}$ normalized by the turbulent Reynolds stress $\overline{u'v'}$ are plotted in figure 15. A positive dimensionless value indicates a downward flux of momentum from this term. Kendall found the wave-induced stress to be downward below the critical height and upward above the critical height. This contradicts the results of Lai & Shemdin, who found large negative contributions to the u, v cospectra (a downward flux) at the wave frequency when U_l/C exceeded unity. With some exceptions, our data support Kendall's measurements. The u, v cospectrum for runs 17–1 and 19–1 were computed and large

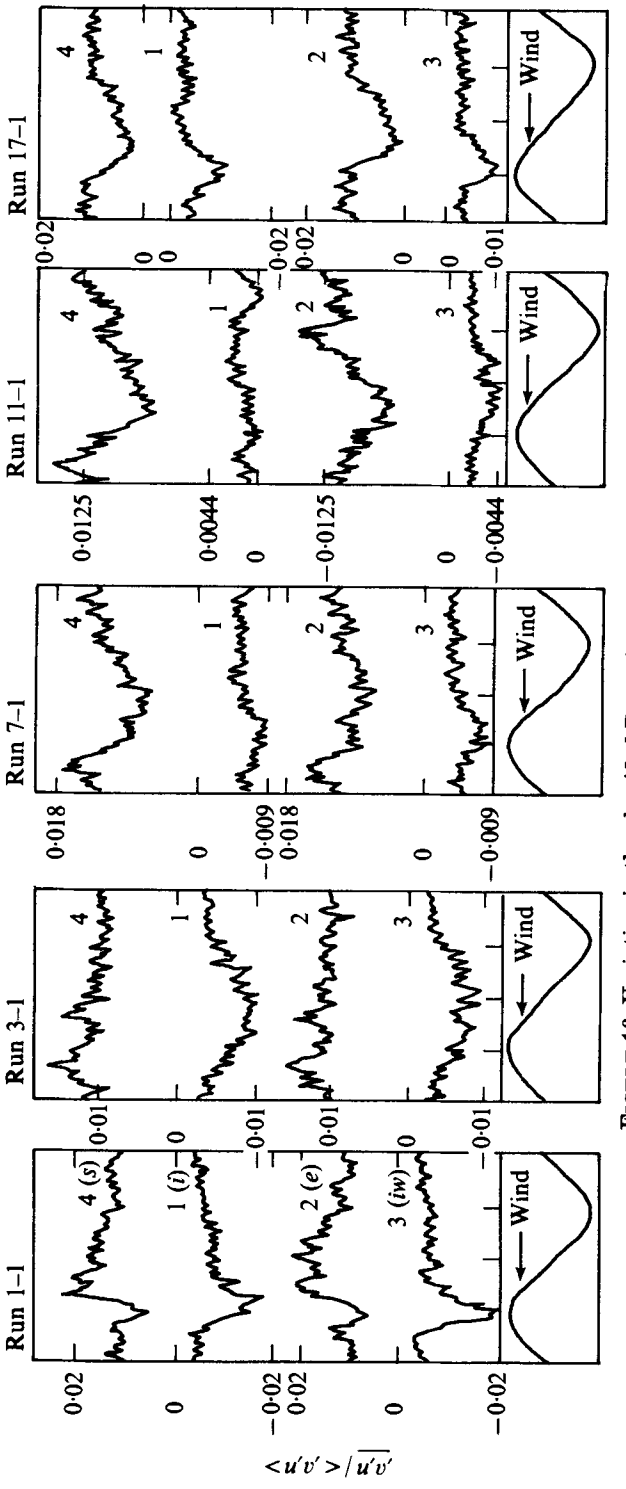

FIGURE 16. Variation in the classified Reynolds stress with wave phase. 1, outward interaction (*i*); 2, ejection (*e*); 3, wallward interaction (*iw*); 4, sweep (*s*).

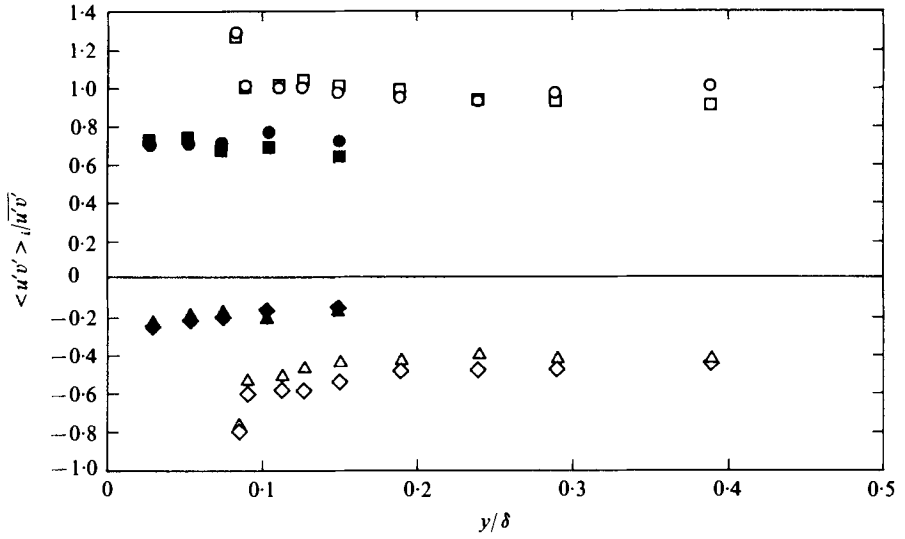

FIGURE 17. Variation in the classified Reynolds stress with height in the boundary layer. Open symbols, data measured over wave; closed symbols, no-wave case. Quadrant: ◇, 1; ○, 2; △, 3; □, 4.

positive peaks were detected at the wave frequency. The observed phase shift between the components was about 50°, v leading u, in agreement with the calculated $\tilde{u}$, $\tilde{v}$ data shown in figures 6–10. It is possible that $\overline{\tilde{u}\tilde{v}}$ is oscillatory in y and that the differences are due to the different wind speeds and heights of the two measurements. Lai & Shemdin's spectra correspond to a wind speed about twice the highest speed used in this experiment. But it is also likely that some of the scatter in our data is due to measurement errors when $\overline{\tilde{u}\tilde{v}}$ is small.

4.3. *Reynolds-stress classification*

The breakdown of the Reynolds stress according to the signs of the u' and v' signals has been extensively studied for smooth-wall shear flows (for example by Lu & Willmarth 1973; Brodkey *et al.* 1974). These studies were motivated by the visual studies of the turbulent boundary layer reported by Kim *et al.* (1971) and Corino & Brodkey (1969), which describe in detail the production of Reynolds stress in the wall region. According to these studies, the Reynolds-stress production is organized and consists of the lifting of low-speed fluid, then oscillatory growth followed by breakup. This entire sequence was termed 'bursting' by Kim *et al.* The bursting events are identified by classification of the measured Reynolds stress according to the signs of u' and v'. Brodkey *et al.* (1974) termed ($u' < 0$, $v' > 0$) an ejection, ($u' > 0$, $v' < 0$) a sweep, ($u' < 0$, $v' < 0$) a wallward interaction and ($u' > 0$, $v' > 0$) an outward interaction.

Figure 16 represents the results of classification of the Reynolds stress according to the signs of u' and v' for five runs. $\langle u'v' \rangle_i$ denotes the phase-averaged ith-quadrant stress. In figure 16 the quadrants correspond to (1) outward interactions, (2) ejections, (3) wallward interactions and (4) sweeps. Quadrants 2 and 4 are the two that contribute to the downward momentum flux. For run 1–1 it is apparent that the negative contribu-

tion to the Reynolds stress at the wave crests occurs because the wallward and outward interactions intensify (positive correlation between u' and v') while the sweeps and ejections are diminished. In run 3–1 the sweeps and ejections do not display any noticeable minimum, but the wallward and outward interactions still display a gradual maximum upwind of the crests and cause the minimum in $\langle u'v' \rangle$. In runs 7–1 and 11–1, however, there are distinct minima in the sweep and ejection quadrants. Finally, in run 17–1 there are minima in the sweeps and ejections coupled with maxima in the wallward and outward interactions upwind of the crests.

The variation of $\overline{\langle u'v' \rangle_i}/\overline{u'v'}$ with height for run 17–1 is shown in figure 17. The fraction of the total time spent in each quadrant was approximately equal, so this plot also represents the contribution of each quadrant to the total stress.

Direct comparison of our data with the smooth-wall results referred to above is difficult because those data were taken in the inner wall region of the flow. However, some comparisons can be made. Our results do agree with Corino & Brodkey's prediction of equal contributions to the total Reynolds stress from ejections and sweeps in the outer part of the boundary layer. Lu & Willmarth (1973) reported that close to the wall approximately 77 % of the total Reynolds stress is due to ejections and 55 % to sweeps. The present results indicate that sweeps and ejections each provide about 100 % of the Reynolds stress while wallward and outward interactions provide about 60 % of the total stress.

The classification procedure was also used on data taken by McIntosh *et al.* over wind waves in the Stanford channel. The results are also shown in figure 17. The free-stream velocity was 3 m s^{-1} and the r.m.s. wave height was 0·14 cm. Flow perturbation by the waves can be considered negligible for these data. The contributions from each quadrant are much lower than for the mechanical-wave data and are consistent with Lu & Willmarth's estimates. The magnitude of the events is enhanced by the presence of the large amplitude wave at least in the outer part of the boundary layer.

5. Summary

The data presented have shown that waves influence the air flow above them. In some cases this influence is obscured by simple time averaging, so that, for example, probability densities and other mean statistics of the flow differed little from those in cases without waves.

Classification of the events (sweeps, ejections, etc. as discussed in § 4.3) producing the turbulent Reynolds stress by the signs of u' and v' showed the events to be more vigorous in the presence of the large amplitude water waves than over flatter surfaces.

The phase-induced velocities $\tilde{u}$ and $\tilde{v}$ did not have simple shapes. The phase of $\tilde{v}$ was a strong function of U_l/C. Variations in $\tilde{u}$ and $\tilde{v}$ with wind speed and height were compatible with the existence of a closed flow about the mean critical height. They were suggestive of an asymmetric 'cat's-eye' pattern, which, as described by Stewart, would result from diffusion of vorticity towards the wave surface. This asymmetric pattern implies that the pressure is out of phase with the wave displacement.

The observed cyclic variation in $\langle u'v' \rangle$ is a result of cyclic variations in the intensity of the turbulent velocity components and not variations in the u', v' correlation.

The wave-induced Reynolds stress $-\overline{\tilde{u}\tilde{v}}$ tends to be positive below the critical height

and negative above. This would appear to contradict Lai & Shemdin's results but agree with Kendall's observations.

This work was supported by the National Science Foundation under Grants Gk-31809X, GA-37534 and ONR N00014-76-C-0155. We wish to thank Professor R. L. Street and Professor E. Y. Hsu for giving us the opportunity to work on this problem and for their review and criticism of the manuscript.

REFERENCES

BENILOV, A. YU., KOUZNETSOV, O. A. & PANIN, G. N. 1974 On the analysis of wind wave-induced disturbances in the atmospheric surface layer. *Boundary-Layer Met.* **6**, 269.

BOLE, J. B. & HSU, E. Y. 1969 Response of gravity water waves to wind excitation. *J. Fluid Mech.* **35**, 657.

BRODKEY, R. S., WALLACE, J. M. & ECKELMANN, H. 1974 Some properties of truncated turbulence signals in bounded shear flows. *J. Fluid Mech.* **63**, 209.

CHANG, P. C., PLATE, E. J. & HIDY, G. M. 1971 Turbulent air flow over the dominant component of wind-generated waves. *J. Fluid Mech.* **47**, 183.

CHAO, S. P. & HSU, E. Y. 1976 Turbulent wind interactions with progressive waves. *Dept. Civil Engng, Stanford Univ. Tech. Rep.* no. 204.

CLAUSER, F. H. 1956 The turbulent boundary layer. *Adv. in Appl. Mech.* vol. 4. Academic Press.

CORINO, E. R. & BRODKEY, R. S. 1969 A visual investigation of the wall region in turbulent flow. *J. Fluid Mech.* **37**, 1.

DAVIS, R. E. 1970 On the turbulent flow over a wavy boundary. *J. Fluid Mech.* **42**, 721.

GUPTA, A. K. & KAPLAN, R. E. 1972 Statistical characteristics of Reynolds stress in a turbulent boundary layer. *Phys. Fluids* **15**, 981.

HSU, E. Y. 1965 A wind water-wave research facility. *Dept. Civil Engng, Stanford Univ. Tech. Rep.* no. 57.

KENDALL, J. M. 1970 The turbulent boundary layer over a wall with progressive surface waves. *J. Fluid Mech.* **41**, 259.

KLEBANOFF, P. S. 1954 Characteristics of turbulence in a boundary layer with zero pressure gradient. *N.A.C.A. Tech. Note* no. 3178.

KIM, H. T., KLINE, S. J. & REYNOLDS, W. C. 1971 Production of turbulence in a boundary layer. *J. Fluid Mech.* **50**, 133.

KONDO, J., FUJINAWA, Y. & NAITO, G. 1972 Wave-induced wind fluctuation over the sea. *J. Fluid Mech.* **51**, 751.

KOVASZNAY, L. S., KIBENS, V. & BLACKWELDER, R. F. 1970 Large-scale motion in the intermittent region of a turbulent boundary layer. *J. Fluid Mech.* **41**, 283.

LAHEY, R. T. & KLINE, S. J. 1971 A stochastic wave model interpretation of correlation functions for turbulent shear flows. *Dept. Mech. Engng, Stanford Univ. Rep.* MD-26.

LAI, R. J. & SHEMDIN, O. H. 1971 Laboratory investigation of air turbulence above simple water waves. *J. Geophys. Res.* **76**, 7334.

LU, S. S. & WILLMARTH, W. W. 1973 Measurements of the structure of the Reynolds stress in a turbulent boundary layer. *J. Fluid Mech.* **60**, 481.

MCINTOSH, D. A., STREET, R. L. & HSU, E. Y. 1975 Turbulent heat and momentum transfer at an air–water interface: the influence of surface conditions. *Dept. Civil Engng, Stanford Univ. Tech. Rep.* no. 197.

NORRIS, H. L. & REYNOLDS, W. C. 1975 Turbulent channel flow with a moving wavy boundary. *Dept. Mech. Engng, Stanford Univ. Tech. Rep.* TF-7.

POND, S., STEWART, R. W. & BURLING, R. W. 1963 Turbulence spectra in the wind over waves. *J. Atmos. Sci.* **20**, 319.

SMITH, S. D. 1967 Thrust-anemometer measurements of wind-velocity spectra and of Reynolds stress over a coastal inlet. *J. Mar. Res.* **25**, 230.

STEWART, R. H. 1970 Laboratory studies of the velocity field over deep-water waves. *J. Fluid Mech.* **42**, 733.

STEWART, R. W. 1974 The air–sea momentum exchange. *Boundary-Layer Met.* **6**, 151.

TAKEUCHI, K. & MOGEL, T. R. 1975 A performance evaluation of a mini-computer. *Rev. Sci. Instr.* **46**, 686.

TENNEKES, H. & LUMLEY, J. L. 1972 *A First Course in Turbulence.* M.I.T. Press.

TOWNSEND, A. A. 1972 Flow in a deep turbulent boundary layer over a surface distorted by water waves. *J. Fluid Mech.* **55**, 719.

YOUNG, M. B. O., HSU, E. Y. & STREET, R. L. 1973 Air–water interaction: the nature of turbulent heat, mass, and momentum transfer mechanisms in the air boundary layer. *Dept. Civil Engng, Stanford Univ. Tech. Rep.* no. 163.